Spontaneous and evoked activity of synaptically coupled neuronal fields with axonal propagation delay for gamma-distributed connectivity kernels

Axel Hutt*
Weierstrass Institute for Applied Analysis and Stochastics,
Mohrenstr.39, 10117 Berlin, Germany
E-mail: hutt@wias-berlin.de

Fatihcan M. Atay
Max-Planck-Institute for Mathematics in the Sciences,
Inselstr. 22, 04103 Leipzig, Germany
E-mail: atay@member.ams.org

Abstract

This work studies dynamical properties of spatially extended neuronal ensembles. We first derive an evolution equation from temporal properties and statistical distributions of synapses and somata. The obtained integro-differential equation considers both synaptic and axonal propagation delay, while spatial synaptic connectivities exhibit gamma-distributed distributions. This familiy of connectivity kernels also covers the cases of divergent, finite, and negligible self-connections. The work derives conditions for both stationary and nonstationary instabilities for gamma-distributed kernels. It turns out that the stability conditions can be formulated in terms of the mean

*Supported by the DFG research center "Mathematics for key technologies" (FZT86) in Berlin, Germany

spatial interaction ranges and the mean spatial interaction times. In addition, a numerical study examines the evoked spatiotemporal response activity caused by short local stimuli and reveals maximum response activity after the mean interaction time at a distance from stimulus offset location equal to the mean interaction range. These findings propose new insights to neuronal mechanisms of experimentally observed evoked brain activity.

1 Introduction

Understanding the basic mechanisms of neuronal activity is supposed to yield insights to major brain functions such as perception, memory processes or motor coordination. The presented work attacks this task by studying spatiotemporal neuronal dynamics caused by fluctuations and environmental external stimuli.

Fluctuations in space and time are always present due to the large number of interconnected neurons and are supposed to be responsible for large-scale coherent phenomena near unstable neural activity states. We mention the phenomena of hallucinations, which frequently result from specific circumstances such as fatigue or sleep deprivation [1] and which, in some cases, exhbits a shift of the neural state to an instability by increased neuronal excitation [2, 3]. For instance, Ermentrout and Cowan [4] introduced a mesoscopical neuronal field theory and explained visual hallucination patterns by loss of stability at bifurcation points.

In contrast, external stimuli may represent sensoric input as auditory speech or visual perceptions. For instance, during cognitive experiments encephalographic measurements reveal coherent evoked brain activity and indicate synchronous neuronal activity on a mesoscopic spatial level [5, 6, 7, 8, 9]. In this context, Freeman [10] has shown in an early work that encephalographic activity relates to mesoscopic dendritic currents. Dipol and current source density models support these findings [11]. Hence, our work aims to study neuronal mechanisms on a spatially mesoscopic level.

Many works studying mesoscopic neuronal activity [12, 13, 14, 15, 16, 17, 18, 19, 20] treat synaptically coupled neuronal ensembles. Our work follows the basic field approach of Jirsa and Haken [5], who combined the ensemble models of Wilson and Cowan [21] and Nunez [22]. This model considers a single type of neurons, which are interconnected by axons terminating at

either excitatory or inhibitory synapses. Though the intrinsic delay due to axonal propagation had been introduced, it does not affect temporal and spatial dynamics. A recent work treating intracortical activity [23, 24] extends the model by introducing synaptic response delay and thus adds a further time scale. It turns out that the relation between synaptic and propagation delay affects the stability of the system. In addition to the temporal scales, the synaptic connectivity kernels define the spatial scales of the neuronal field. In most works, these connectivity kernels exhibit their maximum at zero distances, i.e. strong self-connectivity. Since effects of reduced self-connectivity has not been studied yet in a general form, we shall discuss the family of gamma-distributed connectivity kernels which may exhibit infinite, finite, and negligible probability densities of self-connections for diverse parameters. These cases shall be studied in the context of spontaneous and externally evoked activity.

The paper is organized as follows. The subsequent section presents the derivation of the field equation. In Section 3, stability conditions with respect to spontaneous fluctuations are derived analytically, followed by a numerical study of evoked responses caused by external stimuli. Section 4 summarizes the results and closes the work.

2 Model derivation

The present work treats a three-section model of synaptically coupled neuronal ensembles. Here, one section represents the ensemble set of synapses, which convert the incoming presynaptic activity to postsynaptic potentials (PSP). The adjacent model section contains the ensemble set of trigger zones at somata converting PSPs to axonal pulse activity, while the final one represents the set of axonal fibres linking trigger zones to distant synapses. In the following, these model sections are discussed in some detail.

2.1 Model sections

Chemical synapses convert incoming action potentials to postsynaptic currents by emission of neurotransmitters [25]. Most excitatory synapses (e) emit neurotransmitters called glutamate, which enhance the activity of the postsynaptic cells, while the neurotransmitter γ-aminobutyric (GABA) emitted by inhibitory synapses (i) diminishes the postsynaptic cell activity. In

addition, synapses may bind to dendrites or the soma of the postsynaptic neuron. Hence, the efficacy of synapses is very diverse. While excitatory synapses are often located at dendrites and act faster than inhibitory ones, the latter are often located closer to the soma and thus have larger effects to the neuron.

Furthermore, there is evidence that the dendritic morphology, such as compactness of arborization and branching patterns, affects the stability of connected neurons [14, 26], e.g. due to propagation delays along spatially extended dendrites [27, 28]. In a simplified model, dendrites are electric conductors which exhibit passive spread of current through the dendritic tissue. According to this approach, Freeman [29] was one of the first to show that the response of chemical synapses to incoming action potentials $a(t)$ is approximately equivalent to the convolution of $a(t)$ with an impulse response function $h_{e,i}(t)$. The presented approach accounts for this finding and neglects shunting effects.

In experimental practice single cell activation is measured frequently as the number of action potentials exceeding a certain threshold potential during the time interval $\Delta t \lesssim 2$ms and a sampling procedure at rates $\nu_s \approx 10 - 100$kHz. Hence it is reasonable to assume action potentials at discrete times $t+k/\nu_s,\ k = 1, \ldots, [\nu_s \Delta t]$ and the mean pulse rate at time t gives the number of action potentials in the interval between t and $t+\Delta t$. Here, [..] denotes the nearest integer function. In addition, our model introduces spatial patches $\Gamma(x)$ at location x each containing N synapses, that is, the activity discussed is coarse grained in space. Consequently, postsynaptic potentials averaged over time and space obey

$$\begin{aligned}
\bar{V}^{e,i}(x,t) &= \frac{1}{\Delta t} \sum_{k=1}^{[\nu_s \Delta t]} \frac{1}{N} \sum_{l=1}^{N} g_{e,i}^{(l)} \int_{-\infty}^{t+k/\nu_s} d\tau h_{e,i}(t-\tau) a(x_l, \tau) \\
&\approx \int_{-\infty}^{t} d\tau \; h_{e,i}(t-\tau) \; \frac{1}{\Delta t} \sum_{k=1}^{[\nu_s \Delta t]} \frac{1}{N} \sum_{l=1}^{N} g_{e,i}^{(l)} a(x_l, \tau + k/\nu_s) \\
&= \bar{g}_{e,i} \int_{-\infty}^{t} d\tau \; h_{e,i}(t-\tau) \; \bar{P}_{e,i}(x,\tau) \; , \qquad (1)
\end{aligned}$$

with $x_l \in \Gamma(x)$, $g_{e,i}^{(l)}$ denotes the efficacy of excitatory and inhibitory synapses at location x_l and $\bar{P}_{e,i}(x,t)$ represents the presynaptic pulse rate coarse grained in time and space. Equation (1) assumes presynaptic pulse activity which is fast compared to the slow synaptic response on a time scale of

$5-10$ms. We remark that the replacement of sequences of actual spike trains $a(t)$ is only justified if quantities relevant for the network dynamics are insensitive to trial-to-trial fluctuations, i.e. time coding of spikes is not relevant. This is given in case of uncorrelated single action potentials, which is assumed here. The introduced spatial patches $\Gamma(x)$ represent neuronal assemblies or neuronal pools [13, 21, 22, 30] which build mesoscopic functional entities in the brain and have been found experimentally both in cortical [31, 32] and subcortical [33] areas.

Essentially, we assume variations of synaptic properties in the considered neuronal population [34]. Thus PSPs $V^{e,i}(t)$ at single neurons become random variables with the corresponding probability distributions $p_S^e(V^e - \bar{V}^e)$ and $p_S^i(V^i - \bar{V}^i)$. Since excitatory and inhibitory PSPs sum up at the trigger zone of each neuron [35, 36], the probability density function of the effective membrane potential $V = V^e - V^i$ is

$$p_S(V - \bar{V}) = \frac{1}{2\pi} \int dz \phi_S^e(z) \phi_S^i(-z) e^{-izV} \ , \tag{2}$$

where $\bar{V} = \bar{V}^e - \bar{V}^i$ and ϕ_S^e, ϕ_S^i are the characteristic functions of the corresponding probability density functions of p_S^e, p_S^i.

We now aim to discuss the synaptic properties in more detail. According to [10], the impulse response function from (1) reads

$$h(t) = \frac{\alpha_1 \alpha_2}{\alpha_1 - \alpha_2} (e^{-\alpha_1 t} - e^{-\alpha_2 t}), \qquad \alpha_1, \alpha_2 \ > \ 0 \ .$$

In case of $\alpha_1 = \alpha_2 = \alpha$, the function is the well-known alpha function $h(t) = \alpha^2 t \exp(-\alpha t)$. For maximum impulse response after a delay of ~ 5ms [37], it is $\alpha = 200$Hz. Further, $h(t)$ represents a Green function for the temporal operator

$$\hat{L} = (\frac{\partial}{\partial t} + \alpha_1)(\frac{\partial}{\partial t} + \alpha_2) \tag{3}$$

with $\hat{L}h(t) = \alpha_1 \alpha_2 \delta(t)$ and $\delta(t)$ being the Dirac δ function.

The latter synaptic and dendritic features define the first model section. In the present concept of neuronal ensembles, it converts incoming presynaptic pulse activity to effective somatic membrane potentials.

Now, the adjacent model section focuses on the conversion of membrane potentials to pulse activity. A single neuron generates an action potential

$a(t)$ at time t, i.e. it fires if the membrane potential $V(t)$ at the trigger zone exceeds a certain threshold V_{th}. Thus, the probability of a single neuron to fire is $\Theta(V(t) - V_{th})$, where $\Theta(z)$ denotes the Heaviside function. For an ensemble of neurons at spatial location x, there is a distribution of firing thresholds $D(V_{th} - \bar{V}_{th}, t)$ and thus the expected number of firing neurons is

$$\begin{aligned} N(t) &= \int_{-\infty}^{\infty} dV p_S(V - \bar{V}(t)) \int_{-\infty}^{\infty} dV_{th} \Theta(V - V_{th}) D(V_{th} - \bar{V}_{th}, t) \\ &= \int_{-\infty}^{\infty} dw \int_{-\infty}^{w+\bar{V}(t)-\bar{V}_{th}} du \; p_S(w) D(u, t). \end{aligned}$$

where $\bar{V}_{th}$ denotes the mean firing threshold and p_S is taken from Eq. (2). However, single neurons show refractory time periods and adaption [13, 35], which change the threshold distribution in time. Hence, the time-averaged pulse activity at location x is given by

$$\begin{aligned} \bar{N}(x, t) &= \int_{t}^{t+\Delta t} d\tau \int_{-\infty}^{\infty} dw \; p_S(w) \int_{-\infty}^{w+\bar{V}(x,\tau)-\bar{V}_{th}} du \; D(u, \tau) \\ &\approx \int_{-\infty}^{\infty} dw \; p_S(w) \int_{-\infty}^{w+\bar{V}(x,t)-\bar{V}_{th}} du \; \int_{t}^{t+\Delta t} d\tau D(u, \tau) \\ &= \int_{-\infty}^{\infty} dw \int_{-\infty}^{w+\bar{V}(x,t)-\bar{V}_{th}} du \; p_S(w) \bar{D}(u) \end{aligned} \tag{4}$$

for the time interval Δt sufficiently small and the time-averaged distribution of firing thresholds $\bar{D}(u)$. Here, $\bar{N}(x, t)$ represents the average number of firing neurons in a time interval between t and $t + \Delta t$ in a neuronal ensemble at location x. Since $\bar{N}$ depends on the membrane potential $\bar{V}$, Eq. (4) gives the general definition of the so-called transfer function.

Additionally, the change of pulse activity subject to the membrane potential plays an important role concerning the temporal stability of neuronal ensembles [22, 38] and reads

$$\frac{\partial \bar{N}}{\partial \bar{V}} = \int_{-\infty}^{\infty} dw \; p_S(w) \bar{D}(w + \bar{V} - \bar{V}_{th}). \tag{5}$$

Equations (4) and (5) are general expressions for the well-known sigmoidal conversion and the corresponding conditional pulse probability density or

nonlinear gain [38], respectively, which are subjected to synaptic and somatic statistical properties.
To be more specific, in case of normal-distributed synaptic probability distributions $p_S^{e,i}$, the effective membrane potentials obey a normal distribution $p_S \sim \mathcal{N}(0, \sigma_S^2)$. Additionally, for Gaussian-distributed firing thresholds

$$\bar{D}(u) \;=\; \frac{P_{max}}{\sqrt{2\pi}\sigma_T} e^{-u^2/2\sigma_T^2} \;,$$

the transfer function and nonlinear gain read

$$\begin{aligned} \bar{N}(x,t) &= \frac{P_{\max}}{2}(1+\operatorname{erf}(\frac{\bar{V}(x,t)-\bar{V}_{th}}{\sqrt{2}\sigma})) \\ \frac{\partial \bar{N}(x,t)}{\partial \bar{V}} &= \frac{P_{\max}}{\sqrt{2\pi}\sigma} e^{-(\bar{V}(x,t)-\bar{V}_{th})^2/2\sigma^2}, \end{aligned} \tag{6}$$

respectively, where $\sigma^2 = \sigma_S^2 + \sigma_T^2$, $\operatorname{erf}(x)$ represents the Gaussian error function [39] and P_{max} denotes the maximum firing rate. Equation (6) shows accordance to previous results [40].

The present work approximates the conversion of effective postsynaptic potentials $\bar{V}$ to mean pulse rates $\bar{N}$ from Eq. (6) by the logistic function [29, 38, 41, 42, 43]

$$\bar{N}(x,t) = P_{\max} S(V(x,t)) = \frac{P_{\max}}{1+e^{-c(\hat{V}(x,t)-V_r)}} \tag{7}$$

with parameters c, V_r defined in a later section. Equation (4) gives the major relation of this second model section.

To close the conversion chain of state variables, the final model section contains axonal fibres linking trigger zones and dendritic structures of terminal neurons. In mathematical terms, pulse activity generated at spatial location y propagates along axons by speed $v_{e,i}$ and sums up at terminal excitatory and inhibitory synapses at location x according to the corresponding axonal connectivity distributions $f_e(x,y)$ and $f_i(x,y)$, respectively. More precisely, these distributions are the probability density of axonal connections between two spatial locations x and y. Thereby, the nonlocal interactions yield temporal propagation delays in case of finite axonal propagation speeds. In combination with Eq. (1), this approach is similar to the voltage-based model of Hopfield [44]. Hence, the presynaptic pulse activity reads

$$\bar{P}_{e,i}(x,t) = \int_V dx' f_{e,i}(x,x') \hat{N}(x', t - \frac{|x-x'|}{v_{e,i}}) + \mu_{e,i} I(x,t) \tag{8}$$

with coupling factors $\mu_{e,i}$. The additional pulse activity $I(x,t)$ introduces an external input, e.g. from other cortical regions or from the midbrain [22].

In most previous works [4, 23, 45], neuronal fields exhibit axonal connections which are maximal at zero distance and monotonically decreasing for increasing distance. Then, the combination of excitatory and inhibitory axonal networks may yield four different spatial interactions, namely pure excitation, pure inhibition, local excitation-lateral inhibition and local inhibition-lateral excitation. In contrast, the current work picks up an interestimg result of Nunez [22], who estimated the distribution of axonal cortico-cortical fiber lengths in humans, i.e. the spatial range of excitatory connections, based on distributions in mice. He found that excitatory connections in humans may obey a gamma distribution with maximum at some centimeters. A similar problem has been addressed by Rinzel et al. [46], who found new propagation patterns in inhibitory networks with vanishing self-connections. Since there is also strong anatomical evidence for self-connections in inhibitory networks in cat visual cortex [47], we set the corresponding axonal distribution to a decreasing exponential.

2.2 The field equation

Now, all model sections have been defined and we combine the major results (1), (3), (7) and (8) to

$$\begin{aligned}\hat{L}V(x,t) &= \int_V a_e f_e(x,y) S(V(x', t - \frac{|x-y|}{v_e})) \\ &\quad - a_i f_i(x,y) S(V(y, t - \frac{|x-y|}{v_i}))\ dy + \mu I(x,t)\end{aligned}$$

with $a_{e,i} = \bar{g}_{e,i} P_{\max}$, $\mu = \mu_e - \mu_i$ and

$$f_e(x,y) = \frac{1}{2r_e^p \Gamma(p)} |x-y|^{p-1} e^{-|x-y|/r_e}\ ,\ f_i(x,y) = \frac{1}{2r_i} e^{-|x-y|/r_i} \tag{9}$$

where $p \in \Re,\ p > 0$ is a parameter of the gamma distribution, $\Gamma(p)$ denotes the gamma function and r_e, r_i are the spatial interaction range of excitatory and inhibitory connectivity kernels, respectively. After scaling $t \to t\sqrt{\alpha_1 \alpha_2}, x \to x/r_e, v_{e,i} \to v_{e,i}/(r_e\sqrt{\alpha_1\alpha_2})$ the final field equation reads

$$\hat{L}V(x,t) = \left(\frac{\partial^2}{\partial t^2} + \gamma \frac{\partial}{\partial t} + 1\right) V(x,t)$$

$$= \int_{-\infty}^{\infty} a_e K_e(x-y) S(V(y, t - \frac{|x-y|}{v_e})) - a_i K_i(x-y) S(V(y, t - \frac{|x-y|}{v_i}))dy + \mu I(x,t) \quad (10)$$

with

$$K_e(x) = \frac{1}{2\Gamma(p)} |x|^{p-1} e^{-|x|} \ , \ K_i(x) = \frac{1}{2} r e^{-r|x|} \ , \quad (11)$$

$\gamma = (\alpha + \frac{1}{\alpha}) \geq 2$ and $r = r_e/r_i$. Equation (10) describes the dynamics of a coarse grained field of neuronal ensembles coupled by nonlinear, nonlocal interactions. It is damped by synaptic delay dynamics and subjected to delayed spatial interaction and external input. The mean spatial interaction ranges of excitatory and inhibitory connections, respectively, are given by

$$\xi_e = \int_{-\infty}^{\infty} dx K_e(x)|x| = p, \quad \xi_i = \int_{-\infty}^{\infty} dx K_i(x)|x| = 1/r$$

using Eq. (11). In Figure 1, both kernels are plotted for various parameters p, r and we observe singular local excitations for $p < 1$ (Fig. 1, left panel). At a first glance, this singularity of the probability density K_e may appear unphysical. However, this effect occurs even in much more simple processes and we mention the standard Brownian motion exhibiting a singular probability density of sojourn times [48, 49].

In most works treating spatial structures in neuronal fields, excitatory and inhibitory connectivity kernels are of the same functional type such as exponentials or Gaussians. In these models, the excitation and inhibition comes in by a different sign of the kernel functions and by different spatial scales, say r_e, r_i. In consequence, the spatial interaction ranges can be scaled to $\xi_e = 1$ and $\xi_i \neq 1$. That is, the single parameter ξ_i reflects the relation of the excitatory and the inhibitory spatial scale and defines the spatial interaction. In contrast, Eq. (9) reveals an additional parameter p yielding two variables ξ_e, ξ_i which define the spatial interaction ranges. The additional parameter proposes novel dynamic properties which are extracted in the subsequent sections.

3 Stability analysis

This section aims to study the stability of a stationary state V_0 which is constant in space. In case of constant external input $\mu I(x,t) = I_0$, Eq. (10)

becomes the implicit equation

$$V_0 = (a_e - a_i)S(V_0) + I_0. \tag{12}$$

and Fig. 2 illustrates its different solutions for $a_e > a_i$.

For deviations $u(x,t) = V(x,t) - V_0 = u_0 e^{\lambda t + ikx}$, Eq. (10) reads

$$L(\lambda) = s \int_{-\infty}^{\infty} dz \left(a_e K_e(z) e^{-\frac{\lambda}{v_e}|z|} - a_i K_i(z) e^{-\frac{\lambda}{v_i}|z|} \right) e^{ikz} \tag{13}$$

with the nonlinear gain $s = \delta S / \delta V$ at $V = V_0$.
When $s = 0$, one has $L(\lambda) = \lambda^2 + \gamma\lambda + 1 = 0$, so that $\mathcal{R}\lambda < 0$ and the perturbations u are damped out. It follows that V_0 is asymptotically stable for all small s, since the values (λ, k) satisfying the dispersion relation (13) depend continuously on s. However, increasing s further may result in a loss of stability; in this critical transition one has $\mathcal{R}\lambda = 0$. Thus setting $\lambda = i\omega$ for some $\omega \in \mathbf{R}$ in (13), we get

$$1 - \omega^2 + i\omega\gamma = s \int_{-\infty}^{\infty} dz \left(a_e K_e(z) e^{-i\omega|z|/v_e} - a_i K_i(z) e^{-i\omega|z|/v_i} \right) e^{ikz}. \tag{14}$$

Comparing the magnitudes of both sides,

$$\sqrt{(1-\omega^2)^2 + \gamma^2\omega^2} \leq s \int_{-\infty}^{\infty} dz \left(a_e |K_e(z)| + a_i |K_i(z)| \right). \tag{15}$$

By simple calculus and the fact that $\gamma \geq 2$,

$$(1-\omega^2)^2 + \gamma^2\omega^2 \geq 1 \quad \text{for all } \omega \in \mathbf{R}. \tag{16}$$

Also, by (11),

$$\int_{-\infty}^{\infty} dz |K_{e,i}(z)| = 1. \tag{17}$$

Using (16) and (17) in (15), we obtain the necessary condition for loss of stability

$$1 \leq s(a_e + a_i). \tag{18}$$

In order to investigate the dynamics of the nonlinear equation (10), it is useful to classify the different ways in which V_0 may lose its stability subject to the parameter s in case of spontaneous fluctuations.

3.1 Spontaneous stationary instability

For stationary bifurcations, $\omega = 0$ and the threshold for s becomes

$$s_c = \frac{1}{a_e \hat{K}_e(k_c) - a_i \hat{K}_i(k_c)} = \frac{1}{\hat{K}(k_c)},$$

where $\hat{K}_e$ and $\hat{K}_i$ are the characteristic functions of K_e and K_i, respectively, and

$$\hat{K}(k) = \frac{a_e}{\sqrt{1+k^2}^p} \cos(p \arctan(k)) - a_i r^2 \frac{1}{r^2+k^2}.$$

In case of a constant bifurcation, the stationary state loses stability due to spontaneous fluctuations for

$$s > \frac{1}{\hat{K}(0)} = \frac{1}{a_e - a_i} \ .$$

Figure 3 shows the corresponding bifurcation diagram for various parameters a_e, a_i.

However, increasing s from zero, a non-constant bifurcation may emerge for $(a_e + a_i) > \hat{K}(k_c) > (a_e - a_i)$ with $k_c > 0$ and $a_e > a_i$. The corresponding sufficient condition reads for gamma-distributed kernels

$$\frac{\partial^2 \hat{K}(k)}{\partial k^2}|_{k=0} > 0 \ \Rightarrow \ \xi_i^2 > \frac{a_e}{2a_i} \xi_e(\xi_e + 1) \tag{19}$$

with

$$\frac{\partial^2 \hat{K}(k)}{\partial k^2} = -\frac{a_e p(p+1)}{\sqrt{1+k^2}^{p+2}} \cos((p+2)\arctan(k)) + 2a_i r^2 \frac{r^2 - 3k^2}{(r^2+k^2)^3},$$

which ensures a local maximum of $\hat{K}(k)$ at finite $k_c > 0$, cf. Fig. 4, 5 and 6. The corresponding bifurcation has been found first by Turing in non-equilibrium activator-inhibitor systems [50, 51].

For $\xi_e < 1$, Turing patterns are present for $\xi_i > \xi_e$ (Fig. 5), while for $\xi_e \geq (a_e/a_i)/(2 - a_e/a_i), a_e \leq a_i$ they occur for $\xi_i \leq \xi_e$ as well. This latter case reflects a larger mean excitation range than mean inhibition range and has not been found in previous works. Figure 6 shows the effective kernel $a_e K_e(x) - a_e K_i(x)$ and corresponding Fourier transform $\hat{K}(k)$ for both

$\xi_e = 1$ and $\xi_e = 2.0$. In contrast to kernels with $\xi_e = 1$, which exhibit local excitation-lateral inhibition interaction for $\xi_i > 1$, Turing instabilities may also occur for $\xi_e = 2$ although the kernel elicits local inhibition-lateral excitation interaction.
Eventually recalling the findings of Nunez [22], experiments indicate $\xi_e = 3$ and $a_e > a_i$ for excitatory cortico-cortical connections, i.e. long-range interaction with $r \gg 1$ and thus $\xi_i \ll 1$. According to Eq. (19) and Fig. 4, Turing patterns may not occur for these parameters and also have not been found in experiments.

3.2 Spontaneous non-stationary instability

This type of bifurcation is characterized by a solution pair (λ, k) of (13) with $\lambda = i\omega \neq 0$. We shall show that such bifurcations are possible only if the transmission speeds $v_{e,i}$ are not too large, and obtain an estimate to quantify this statement.

Considering the imaginary part of (14),

$$\begin{aligned}\omega\gamma &= -s\int_{-\infty}^{\infty} dz\,(a_e K_e(z)\sin(\omega|z|/v_e) - a_i K_i(z)\sin(\omega|z|/v_i))\cos(kz)\\ &\quad +s\int_{-\infty}^{\infty} dz\,(a_e K_e(z)\cos(\omega|z|/v_e) - a_i K_i(z)\cos(\omega|z|/v_i))\sin(kz).\end{aligned}$$

Note that the integrand in the first integral is an even function of z while that in the second integral is an odd function. Thus the second integral vanishes, and we have

$$\omega\gamma = -2s\int_0^{\infty} dz\,(a_e K_e(z)\sin(\omega z/v_e) - a_i K_i(z)\sin(\omega z/v_i))\cos(kz)$$

which yields

$$|\omega|\gamma \leq 2s\int_0^{\infty} dz\,(a_e|K_e(z)\sin(\omega z/v_e)| + a_i|K_i(z)\sin(\omega z/v_i)|)\,.$$

Using the fact that $|\sin x| \leq |x|$ for all x, we obtain

$$|\omega|\gamma \leq 2s\int_0^{\infty} dz\,(a_e|K_e(z)\omega z/v_e| + a_i|K_i(z)\omega z/v_i|)$$

and since $\omega \neq 0$ at a non-stationary bifurcation,

$$\gamma \leq s\left(\frac{a_e}{v_e}\int_0^{\infty} dz\,2K_e(z)z + \frac{a_i}{v_i}\int_0^{\infty} dz\,2K_i(z)z\right).$$

Note that the integrals are the definitions of the mean spatial interaction ranges ξ_e and ξ_i for excitatory and inhibitory connections, respectively. Hence we define

$$\tau_e = \frac{1}{v_e}\int_{-\infty}^{\infty} dz\, K_e(z)|z| = \xi_e/v_e, \quad \tau_i = \frac{1}{v_i}\int_{-\infty}^{\infty} dz\, K_i(z)|z| = \xi_i/v_i \qquad (20)$$

as the mean delay times respectively for the excitatory and inhibitory information transmission in the field. In this way, we can express a necessary condition for non-stationary bifurcations to occur, namely

$$s \geq s_c = \frac{\gamma}{a_e\tau_e + a_i\tau_i}. \qquad (21)$$

Since all quantities are positive, it is clear that at least one of the velocities v_e or v_i must be finite for the occurence of non-stationary bifurcations. For the particular case when the distributions are given by (11), we have

$$\frac{\gamma}{s} \leq \frac{a_e p}{v_e} + \frac{a_i/r}{v_i}$$

by using the mean values of the gamma and exponential probability density distributions. This relation elicits a decreased threshold s_c for increased values of p and $1/r$, i.e. the larger p and $1/r$ the easier nonstationary bifurcations may occur.

With Eq. (21) and the previous condition $1/(a_e + a_i) < s < 1/(a_e - a_i)$ for nonconstant bifurcations , the parameter regime for nonstationary bifurcation is given by

$$\frac{\gamma}{\tau_e\frac{a_e}{a_i} + \tau_i} < a_i s < \frac{1}{\frac{a_e}{a_i} - 1} \quad , \quad \frac{1}{\frac{a_e}{a_i} + 1} < a_i s$$

As can be shown by simple calculus, there is a threshold

$$a_e/a_i = \frac{\gamma + \tau_i}{\gamma - \tau_e} \quad , \quad \tau_e < \gamma$$

beyond which no nonstationary bifurcations occur, while $\tau_e > \gamma$ allows nonstationary bifurcations for all $a_e/a_i \geq 1$. Figure 7 illustrates these findings.

3.3 Evoked stimulus response

Finally, we study Eq. (10) numerically and aim to extract its spatiotemporal properties for different excitatory spatial ranges ξ_e. In experimental practice, neural tissue is stimulated by local external input during a finite time interval. We choose the external stimulus to be

$$I(x,t) = I_0 + \begin{cases} I_{local} & : \quad x_0 \leq x \leq x_0 + \Delta x \ , \ 0 \leq t \leq \Delta T \\ 0 & : \quad \text{otherwise} \end{cases}$$

For the numerical investigations parameters are chosen to be physiologically reasonable as $c = 1.8, V_r = 3.0$ [52] and $\alpha_1 = \alpha_2 = 200\text{Hz}$ [37, 43], i.e. $\gamma = 2$. From [22], we obtain spatial ranges $r_e = 20\text{mm}$, $r_i \approx 1\text{mm}$, i.e. $\xi_i = 0.05$, and $\xi_e = 3$. The spatial field exhibits 400 discrete elements each of length $dx = 1\text{mm}$, while the time period is discretized by 100 time steps each of duration $dt = 0.4\text{ms}$. In addition, the propagation speed along excitatory axonal connections is $v_e = 8\text{m/s}$, while the delay corresponding to short-range inhibitory connections is neglected.

The subsequent temporal integration procedure applies an Euler algorithm while the spatial integration algorithm obeys

$$\int_0^L f(z)dz \approx \sum_{i=1}^{N} \frac{1}{2}(f(z_i) + f(z_{i+1}))\ dx \tag{22}$$

for an integrand f, here with $N = 400$ and $L = 400\text{mm}$. Furthermore, periodic boundary conditions are set, yielding

$$\int_{-\infty}^{\infty} K(|x-y|)f(y)dy \approx \int_0^L K(L/2 - |L/2 - |x-y||)f(y)dy.$$

Initial values $V^0(x,t) = V_0$ for $-L/v_e \leq t \leq 0$ guarantee negligible initial transients. For synaptic parameters $a_e = 25, a_i = 5$ and constant external stimulus $I_0 = 0.1$, it is $V_0 = 0.23$ and the condition (18) for asymptotic stability holds. The additional local stimulus of strength $I_{local} = 5$, width $\Delta x = 10\text{mm}$ and duration $\Delta T = 8\text{ms}$ evokes spatiotemporal activity, which is shown as space-time plots in Fig. 8 for various excitatory spatial ranges $\xi_e = p$. During stimulation no activity spreads into the field, while after stimulus offset activation travels from the stimulus center. Graphical evaluations reveal that the activation propagates with the axonal speed v_e and exhibits its maximum at a distance $\xi_e \cdot r_e$ from stimulus offset location, i.e. at the

mean excitatory interaction range. Hence, the expected time for maximum stimulus response is the mean interaction time τ_e from Eq. (20). These findings coincide for all parameters $\xi_e = p$ in Fig. 8. Though further analytical examinations are necessary to validate these first numerical findings, they would exceed the major aim of the paper and shall be discussed in future work.

Finally, we examine the activity response evoked by a different stimulus

$$I(x,t) = I_0 + \begin{cases} 5.0 \cdot \cos(k_0 x) & : \quad 0 \leq t \leq \Delta T \\ 0 & : \quad \text{otherwise} \end{cases}$$

for the same parameters as above. Figure 9 shows results for (a) $k_0 = 2\pi/20\,\mathrm{mm}^{-1}$ and (b) $k_0 = 2\pi/200\,\mathrm{mm}^{-1}$. We observe diverse periodic spatiotemporal patterns, which reveal the spatial periodicity of the stimulus and the mean excitatory interaction time.

4 Conclusion

The present work introduces a three-section model for non-local interacting neuronal ensembles. It considers synaptic and axonal propagation delay effects besides general gamma-distributed excitatory and inhibitory axonal connectivities. In a derivation step, a general somatic transfer function is derived from statistical synaptic and somatic properties. The obtained field equation is studied with respect to its stability towards spontaneous fluctuations and external stimuli. Conditions for Turing and nonstationary instabilities exhibit only a few parameters. That is, mean excitatory and inhibitory spatial interaction ranges define the sufficient parameter regime of spontaneous Turing patterns, while mean excitatory and inhibitory interaction times determine the necessary parameter regime of spontaneous nonstationary phenomena. Interestingly, these parameters also appear to play an important role in the evoked response activity caused by local external stimuli. In the numerical study, evoked activation propagates at axonal propagation speed and its maximum occurs at a distance from stimulus onset equal to the mean spatial interaction range after the corresponding mean interaction time. This rather intuitive finding gives new insights to stimulus responses in nonlocally interacting fields and, especially, to information processing in local brain areas during cognitive processing of external stimuli.

Future work will discuss evoked responses analytically subjected to diverse stationary and nonstationary spatiotemporal stimuli.

Acknowledgements

The authors thank T.Wennekers for valuable hints and for reading the manuscript.

References

[1] J. R. Brasic, Hallucinations, Percep. Motor Skills 86 (1998) 851

[2] S. H. Isaacson, J. Carr, A. J. Rowan, Cibroflocacin-induced complex partial status epilepticus manifesting as an acute confusional state, Neurol. 43 (1993) 1619

[3] P. Tass, Oscillatory cortical activity during visual hallucinations, J. Biol. Phys. 23 (1997) 21

[4] G. B. Ermentrout, J. D. Cowan, A mathematical theory of visual hallucination patterns, Biol. Cybern. 34 (1979) 137

[5] V. K. Jirsa, H. Haken, Field theory of electromagnetic brain activity, Phys. Rev. Lett. 7 (5) (1996) 960

[6] C. Uhl (Ed.), Analysis of Neurophysiological Brain Functioning, Springer-Verlag, Berlin, 1999.

[7] A. Hutt, H. Riedel, Analysis and modeling of quasi-stationary multivariate time series and their application to middle latency auditory evoked potentials, Physica D 177 (2003) 203

[8] H. Haken, Principles of Brain Functioning, Springer, Berlin, 1996.

[9] W. J. Freeman, Neurodynamics: An Exploration in Mesoscopic Brain Dynamics (Perspectives in Neural Computing), Springer-Verlag, Berlin, 2000.

[10] W. J. Freeman, A model for mutual excitation in a neuron population in olfactory bulb, IEEE Trans. Biomed. Engin. 21 (1974) 350

[11] J. C. Mosher, P. S. Lewis, R. M. Leahy, Multiple dipol modeling and localization from spatio-temporal meg-data, IEEE Trans. Biomed. Eng. 39 (6) (1992) 541

[12] P. A. Robinson, P. N. Loxley, S. C. O'Connor, C. J. Rennie, Modal analysis of corticothalamic dynamics, electroencephalographic spectra and evoked potentials, Phys. Rev. E 63 (2001) 041909.

[13] W. Gerstner, Time structure of the activity in neural network models, Phys. Rev. E 51 (1) (1995) 738

[14] P. Bressloff, S. Coombes, Physics of the extended neuron, Int. J. Mod. Phys. B 11 (20) (1997) 2343

[15] B. Ermentrout, Neural networks as spatio-temporal pattern-forming systems, Rep. Prog. Phys. 61 (1998) 353

[16] W. M. Kistler, R. Seitz, J. L. van Hemmen, Modeling collective excitations in cortical tissue, Physica D 114 (1998) 273

[17] R. Ben-Yishai, R. L. Bar-Or, H. Sompolinsky, Theory of orientation tuning in visual cortex, Proc. Natl. Acad. Sci. 92 (1995) 3844

[18] T. Wennekers, Dynamic approximation of spatio-temporal receptive fields in nonlinear neural field models, Neural Comp. 14 (2002) 1801

[19] K. J. Friston, Transients, metastability and neuronal dynamics, NeuroImage 5 (1997) 164

[20] J. Eggert, J. L. van Hemmen, Unifying framework for neuronal dynamics, Phys. Rev. E 61 (2) (2000) 1855

[21] H. R. Wilson, J. D. Cowan, Excitatory and inhibitory interactions in localized populations of model neurons, Biophys. J. 12 (1972) 1

[22] P. L. Nunez, Neocortical dynamics and human EEG rhythms, Oxford University Press, New York - Oxford, 1995.

[23] A. Hutt, M. Bestehorn, T. Wennekers, Pattern formation in intracortical neuronal fields, Network: Comput. Neural Syst. 14 (2003) 351

[24] F. M. Atay, A. Hutt, Stability and bifurcations in neural fields with axonal delay and general connectivity, Preprint 857, Weierstrass-Institute Berlin, Germany (2003).

[25] J. C. Eccles, M. Ito, J. Szentagothai, The Cerebellum as a Neuronal Machine, Springer-Verlag, New York, 1967.

[26] P. S. Katz, W. N. Frost, Intrinsic neuromodulation: altering neuronal circuits from within, Trends Neurosci. 19 (1996) 54

[27] W. Rall, Theory of physiological properties of dendrites, Ann. N.Y. Acad. Sci. 96 (1962) 1071

[28] W. Rall, Cable properties of dendrites and effects of synaptic location, in: P. Andersen, J. K. S. Jansen (Eds.), Excitatory Synaptic Mechanisms, Universitetsforlaget, Oslo, Norway, 1970, pp. 175

[29] W. J. Freeman, Mass Action in the Nervous System, Academic Press, New York, 1975.

[30] J. Eggert, J. L. van Hemmen, Modeling neuronal assemblies: Theory and implementation, Neural Comput. 13 (9) (2001) 1923

[31] V. B. Mountcastle, Modality and topographic properties of single neurons of cat's somatic sensory cortex., Neurophysiol. 20 (1957) 408

[32] D. H. Hubel, T. N. Wiesel, Receptive fields of cells in striate cortex of very young, visually unexperienced kittens, J. Physiol 26 (1963) 994

[33] K. J. Sanderson, The projection of the visual field to the lateral geniculate and medial interlaminar nuclei in the cat, J. Comp. Neurol. 143 (1971) 101

[34] B. Katz (Ed.), Nerve, Muscle and Synapse, McGraw-Hill, New York, 1966.

[35] W. J. Freeman, Tutorial on neurobiology: from single neurons to brain chaos, Int. J. Bif. Chaos 2 (3) (1992) 451

[36] W. J. Freeman, Characteristics of the synchronization of brain activity imposed by finite conduction velocities of axons, Int. J. Bif. Chaos 10 (10) (2000) 2307

[37] F. H. L. da Silva, A. Hoeks, A. Smits, L. H. Zetterberg, Model of brain rhythmic activity, Kybernetik 15 (1974) 24

[38] W. J. Freeman, Nonlinear gain mediating cortical stimulus-response relations, Biol. Cybern. 33 (1979) 237

[39] E. Zeidler (Ed.), Teubner-Taschenbuch der Mathematik, Teubner-Verlag, Leipzig, 1996.

[40] D. J. Amit, Modeling brain function: The world of attactor neural networks, Cambridge University Press, Cambridge, 1989.

[41] W. A. Little, The existence of persistent states in the brain, Math. Biosc. 19 (1974) 101

[42] J. J. Wright, D. T. J. Liley, Simulation of electrocortical waves, Biol. Cybern. 72 (1995) 347

[43] P. A. Robinson, C. J. Rennie, J. J. Wright, Propagation and stability of waves of electrical activity in the cerebral cortex, Phys. Rev. E 56 (1) (1997) 826

[44] J. Hopfield, Neurons with graded response have collective computational properties like those of two-state neurons, Proc. Nat. Acad. Sci. 81 (1984) 3088

[45] H. R. Wilson, J. D. Cowan, A mathematical theory of the functional dynamics of cortical and thalamic nervous tissue, Kybernetik 13 (1973) 55

[46] J. Rinzel, D. Terman, X. J. Wang, B. Ermentrout, Propagating activity patterns in large-scale inhibitory neuronal networks, Science 279 (1998) 1351

[47] G. Tamas, E. H. Buhl, P. Somogyi, Massive autaptic self-innervation of gabaergic neurons in cat visual cortex, J. Neurosci. 17 (16) (1997) 6352

[48] P. Levy, Sur certains processus stochastique homogènes, Comp. Math. 7 (1939) 283

[49] W. Feller, An introduction to probability theory and its applications, Wiley, New York, 1966.

[50] A. Turing, The chemical basis of morphogenesis, Philos. Trans. R. Soc. London 327B (1952) 37

[51] V. Castets, E. Dulos, J. Boissonade, P. D. Kepper, Experimental-evidence of a sustained standing turing-type non-equilibrium chemical-pattern, Phys. Rev. Lett. 64 (1990) 2953

[52] J. J. Wright, D. T. J. Liley, A millimetric-scale simulation of electrocortical wave dynamics based on anatomical estimates of cortical synaptic density, Biosyst. 63 (2001) 15

Figure 1: Excitatory and inhibitory kernels for various parameters. All kernels are finite except for $K_e(x)$ for $p = 0.5$. In case of $p > 1$, kernel $K_e(x)$ exhibits a maximum far from the origin.

Figure 2: Illustration for the detection of constant stationary solutions of Eq. (12). For $I_0 < 1.32$, there are three solutions, while for $I_0 > 1.32$ there is only a single one at large values of V_0. Simple iteration studies near the solutions reveal their stability: filled circles represent stable fixed points, while empty circles illustrate unstable fixed points. At the critical value $I = 1.32$, there is a saddle node solution (hatched circle) synchronous to a stable fixed point at large values of V_0, cf. Fig. 3. Here, $a_e = 10, a_i = 5$ and $c = 1.8,\ V_r = 3.0$ [52].

Figure 3: Bifurcation diagram and nonlinear gain for constant bifurcations for $a_e > a_i$. Left panel: stability of the stationary state V_0 with respect to external input I_0. For $a_e - a_i > 4/c = 2.22$, both stable (solid line) and unstable branches (dashed line) exist, while for $a_e - a_i \leq 2.22$ there is only a single stable solution. Right panel: the nonlinear gain s with respect to the constant state V_0. The horizontal line $s = 1/(a_e - a_i)$ separates stable from unstable states and determines the critical values of V_0. In both panels, $c = 1.8,\ V_r = 3.0$.

Figure 4: Parameter regimes of Turing patterns for spatial interaction ranges ξ_i and ξ_e and various values of $a_e/a_i > 1$. The thin solid line denotes $\xi_i = \xi_e$, while filled and empty squares, triangles and diamonds mark different cases discussed in Fig. 5 and Fig. 6.

Figure 5: Function $\hat{K}(k)$ for $\xi_e < \xi_i$. Parameter values are chosen according to Fig. 4. Both values of ξ_e allow a local maximum of $\hat{K}(k)$ for $k > 0$ and thus facilitates Turing patterns. Here, $a_e = 10, a_i = 5$.

Figure 6: The kernel function $a_e K_e(x) - a_i K_i(x)$ and the function $\hat{K}(k)$ for $\xi_e \geq \xi_i$. Parameter values are chosen according to Fig. 4. In case of $\xi_e = 1.0$, local excitation-lateral inhibition ($\xi_i = 1.10$) yields a local maximum of $\hat{K}$, i.e. Turing patterns, while local inhibition-lateral excitation ($\xi_i = 0.90$) prohibits Turing patterns. In constrast, $\xi_e = 2.0$ exhibits local inhibition-lateral excitation for both values of ξ_i, while $\hat{K}$ shows a local maximum for $\xi_i = 1.96$. Here, $a_e = 10, a_i = 5$.

Figure 7: Necessary parameter regime for nonstationary instabilities for diverse mean excitatory interaction time τ_e and synaptic delay constant γ. Valid parameters (hatched area) are constrained by the threshold of Eq. (21) plotted as solid line, the threshold of constant bifurcation (dotted line) and the threshold of asymptotic stability (dashed line).

Figure 8: Spatiotemporal stimulus response to a local stimulation for various parameters $\xi_e = p$. Left column: Space-time plots of field activity, while the greyscale encodes positive (white) and negative (black) deviations from the stationary state (grey). The activity V has been clipped for $|V - V_0| > 0.05$ due to illustrative reasons, i.e. equal-greyscaled areas occur due to clipping. Activity propagation speeds are computed for all p along estimated lines which are similar to the dashed line plotted for $p = 3$. Right column: several time samples of spatial activity for the corresponding values of p.

Figure 9: Spatiotemporal stimulus response to a spatially periodic stimulus. The greyscale encoding is the same as in Fig. 8.

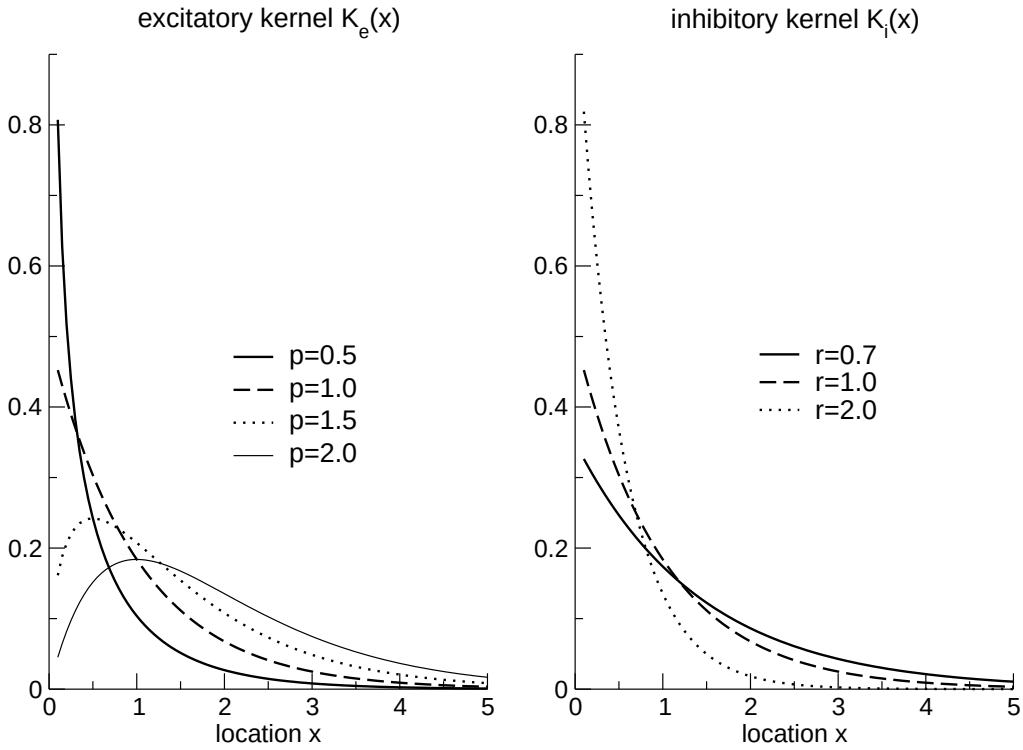
excitatory kernel $K_e(x)$
inhibitory kernel $K_i(x)$
0.8
0.6
0.4
0.2
0
0
1
2
3
4
5
location x
p=0.5
p=1.0
p=1.5
p=2.0
r=0.7
r=1.0
r=2.0

Figure 1

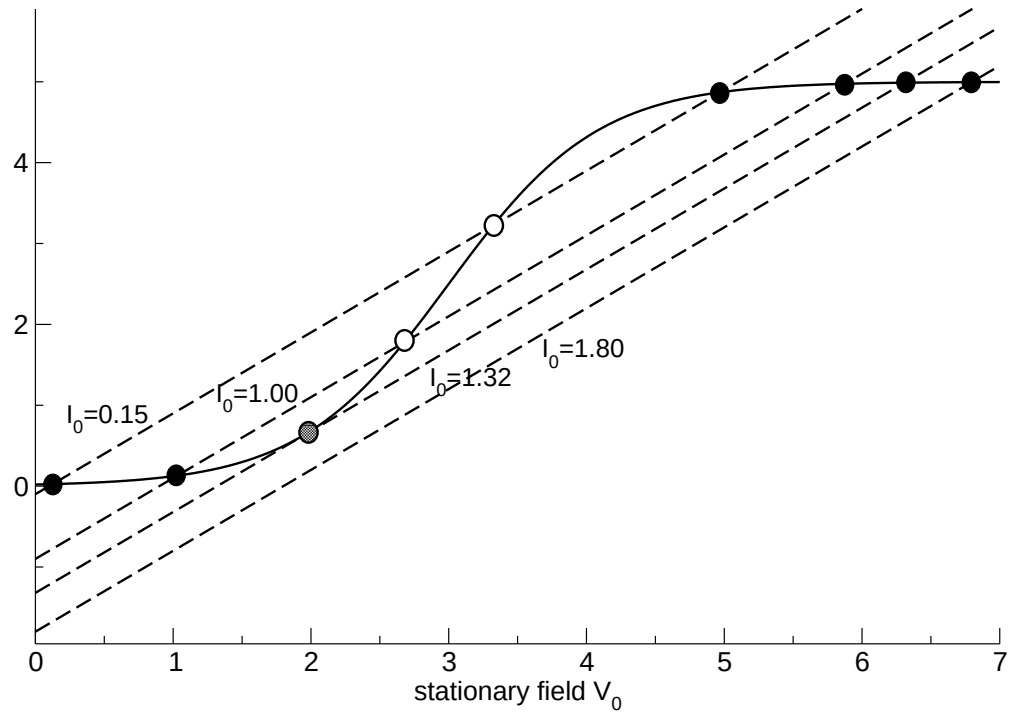

Figure 2

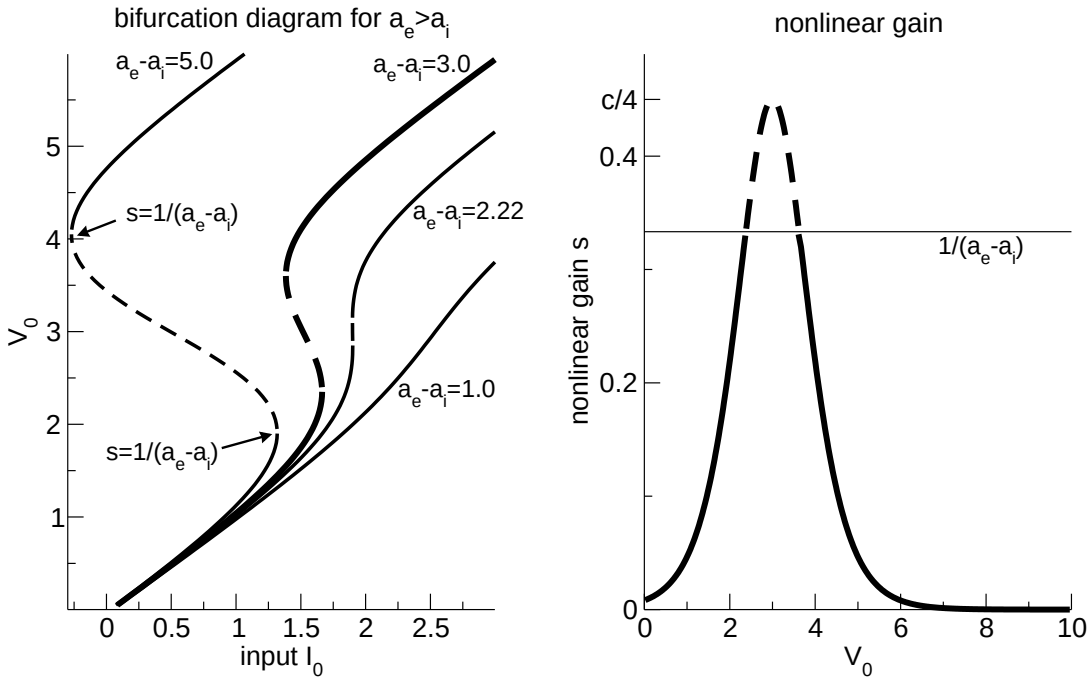
bifurcation diagram for $a_e > a_i$
$a_e - a_i = 5.0$
$a_e - a_i = 3.0$
$a_e - a_i = 2.22$
$a_e - a_i = 1.0$
$s = 1/(a_e - a_i)$
$s = 1/(a_e - a_i)$
V_0
input I_0
0
0.5
1
1.5
2
2.5
1
2
3
4
5
nonlinear gain
c/4
0.4
0.2
0
nonlinear gain s
$1/(a_e - a_i)$
0
2
4
6
8
10
V_0

Figure 3

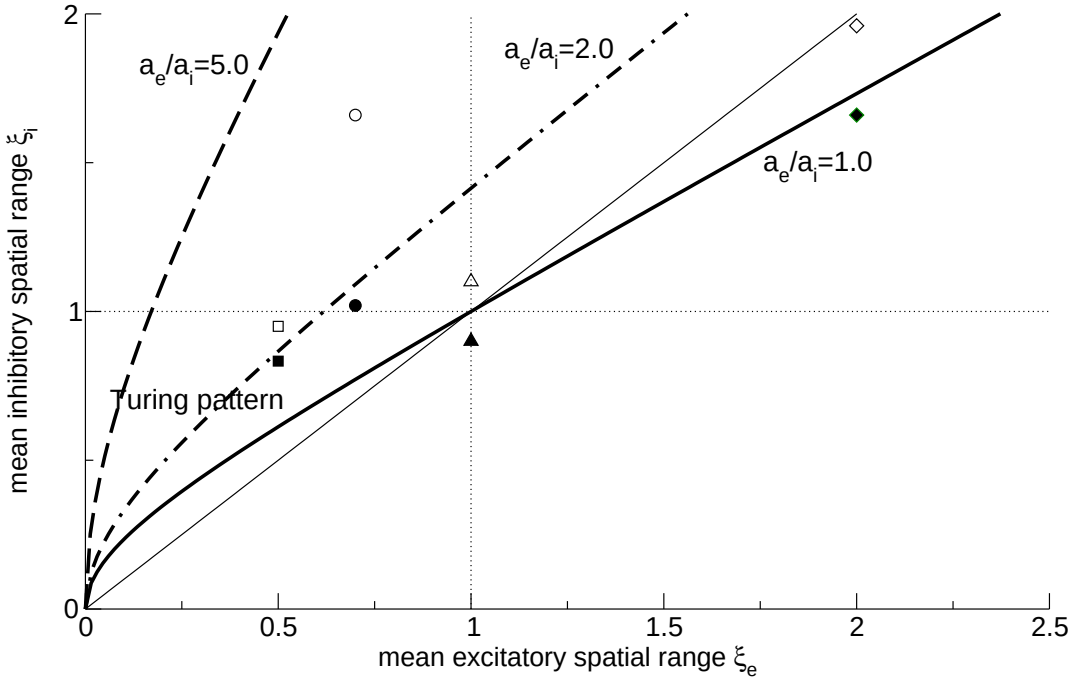
2
1
0
0
0.5
1
1.5
2
2.5
mean inhibitory spatial range ξi
mean excitatory spatial range ξe
ae/ai=5.0
ae/ai=2.0
ae/ai=1.0
Turing pattern

Figure 4

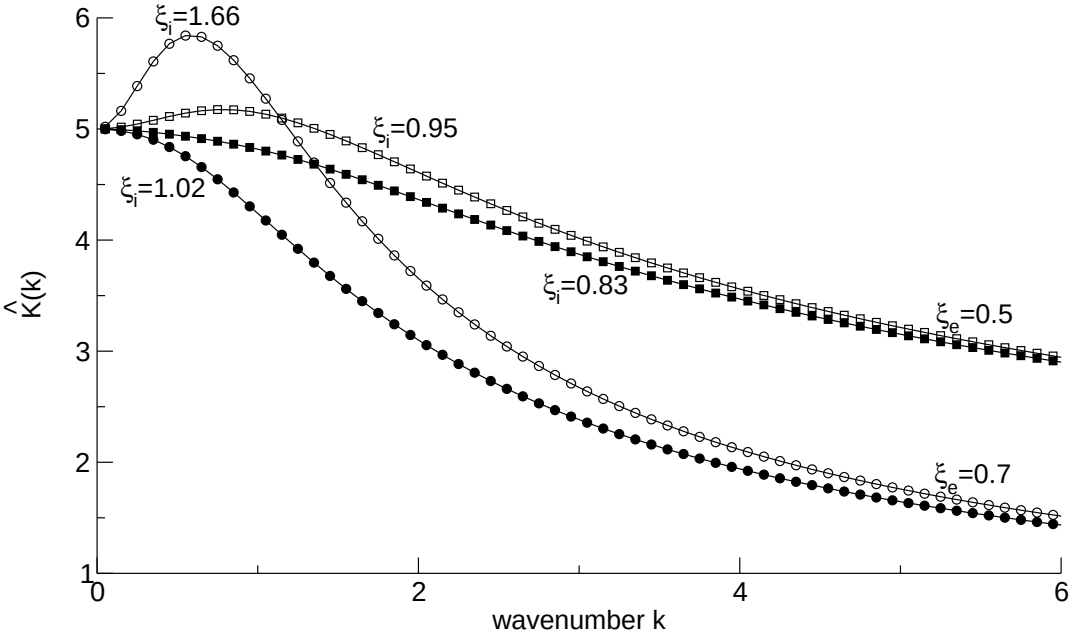
ξi=1.66
ξi=0.95
ξi=1.02
ξi=0.83
ξe=0.5
ξe=0.7
K̂(k)
wavenumber k
0
2
4
6
1
2
3
4
5
6

Figure 5

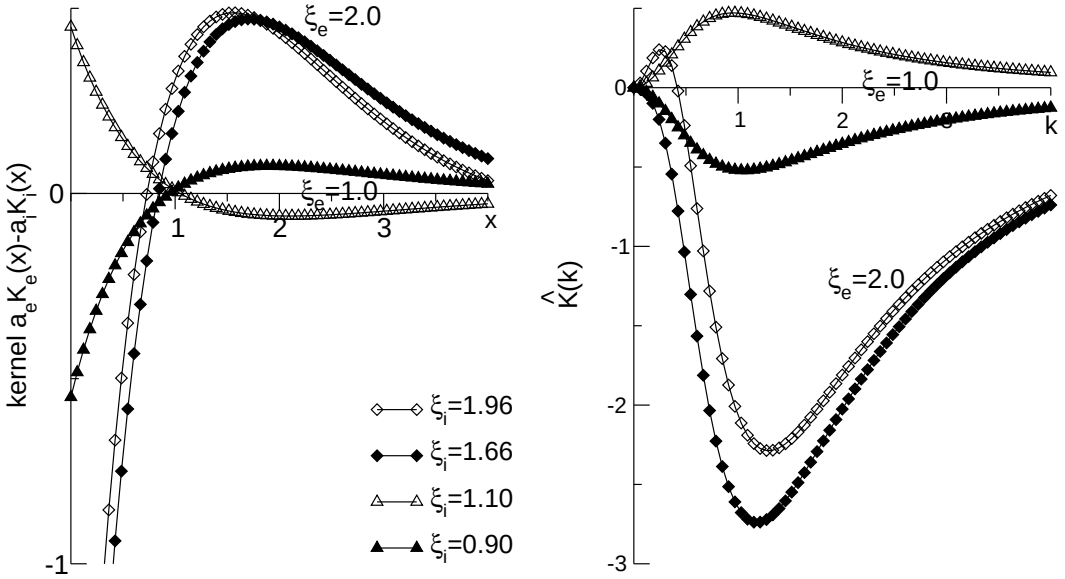
ξe=2.0
ξe=1.0
kernel aeKe(x)-aiKi(x)
0
1
2
3
x
-1
ξi=1.96
ξi=1.66
ξi=1.10
ξi=0.90
K̂(k)
0
1
2
3
k
-1
-2
-3
ξe=1.0
ξe=2.0

Figure 6

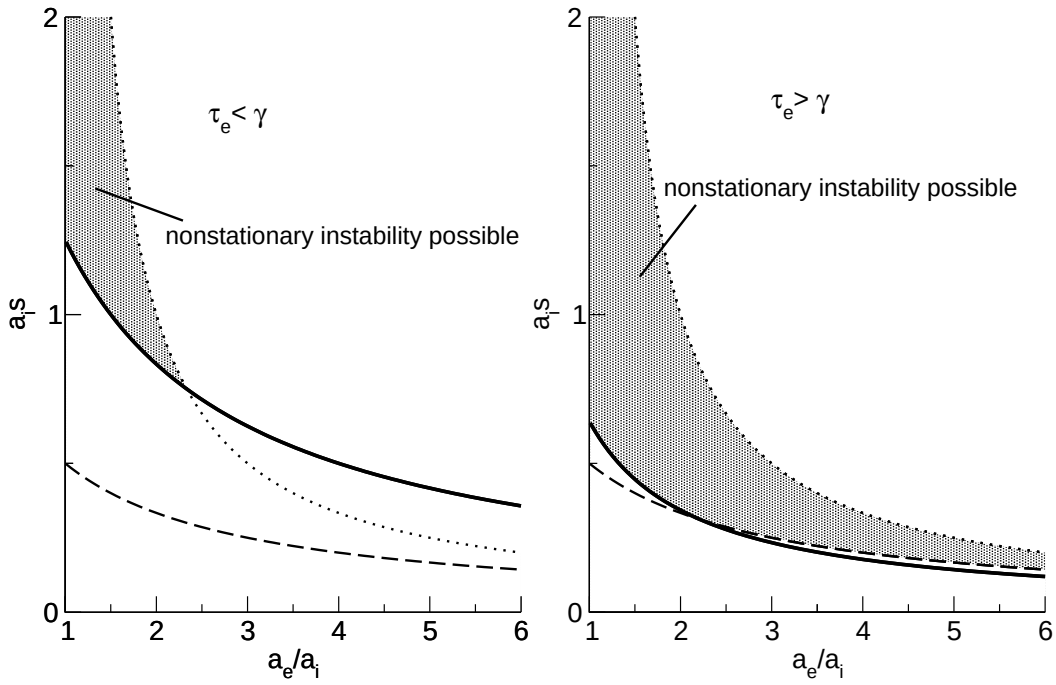
2
1
0
$a_i s$
$\tau_e < \gamma$
nonstationary instability possible
1
2
3
4
5
6
a_e/a_i
2
1
0
$a_i s$
$\tau_e > \gamma$
nonstationary instability possible
1
2
3
4
5
6
a_e/a_i

Figure 7

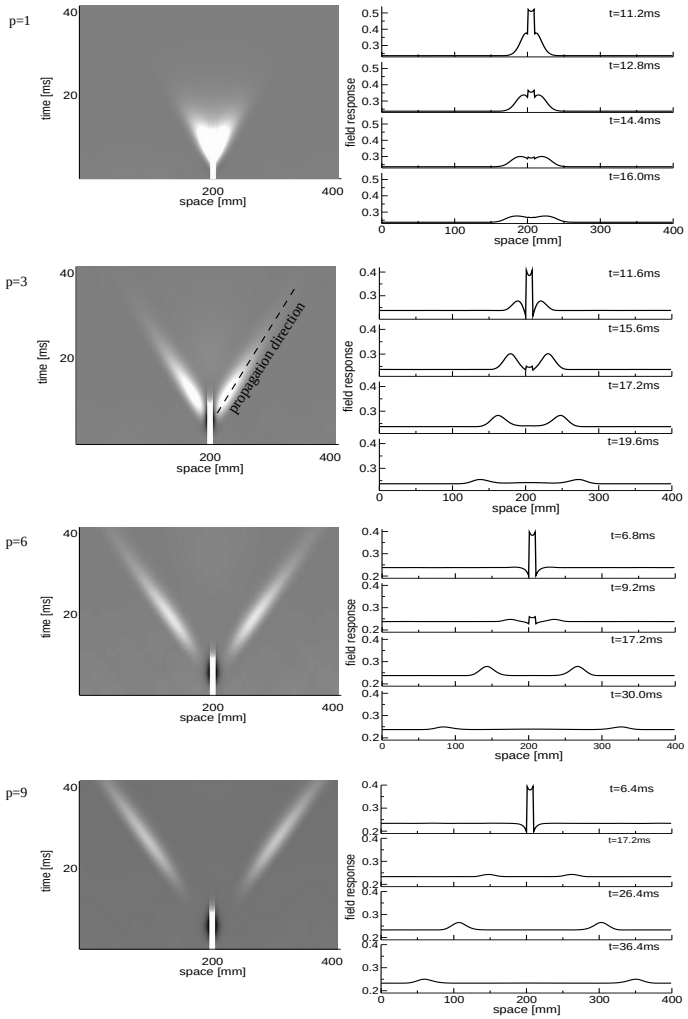
p=1
time [ms]
space [mm]
field response
t=11.2ms
t=12.8ms
t=14.4ms
t=16.0ms
p=3
propagation direction
t=11.6ms
t=15.6ms
t=17.2ms
t=19.6ms
p=6
t=6.8ms
t=9.2ms
t=17.2ms
t=30.0ms
p=9
t=6.4ms
t=17.2ms
t=26.4ms
t=36.4ms

Figure 8

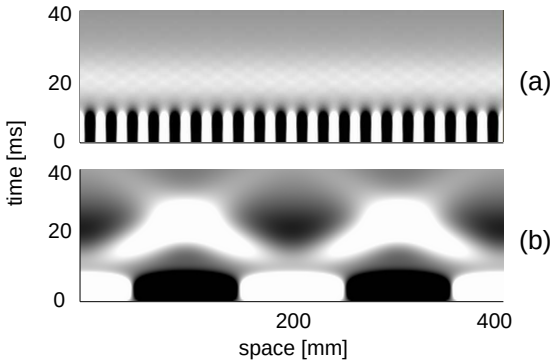

Figure 9